Supporting Information for

Aging of Self-Assembled Lead Halide Perovskite Nanocrystal Superlattices: Effects on Photoluminescence and Energy Transfer

Dmitry Baranov*,[1] Antonio Fieramosca,[2,3†] Ruo Xi Yang,[4] Laura Polimeno,[2,3] Giovanni Lerario,[2] Stefano Toso,[1,5] Carlo Giansante,[2] Milena De Giorgi,[2] Liang Z. Tan*,[4] Daniele Sanvitto*,[2] Liberato Manna*[1]

[1]Nanochemistry Department, Italian Institute of Technology, Via Morego 30, Genova 16163, Italy;
[2]CNR Nanotec, Institute of Nanotechnology, Via Monteroni, Lecce 73100, Italy
[3]Dipartimento di Matematica e Fisica "E. de Giorgi," Università Del Salento, Campus Ecotekne, via Monteroni, Lecce 73100, Italy
[4]Molecular Foundry, Lawrence Berkeley National Lab, Berkeley, California 94720, USA
[5]International Doctoral Program in Science, Università Cattolica del Sacro Cuore, Brescia 25121, Italy;

[†] – present address: Division of Physics and Applied Physics, School of Physical and Mathematical Sciences, Nanyang Technological University, Singapore 637371, Singapore

* – corresponding authors: dmitry.baranov@iit.it, lztan@lbl.gov, daniele.sanvitto@nanotec.cnr.it, liberato.manna@iit.it

Contents

S1. Supplemental figures

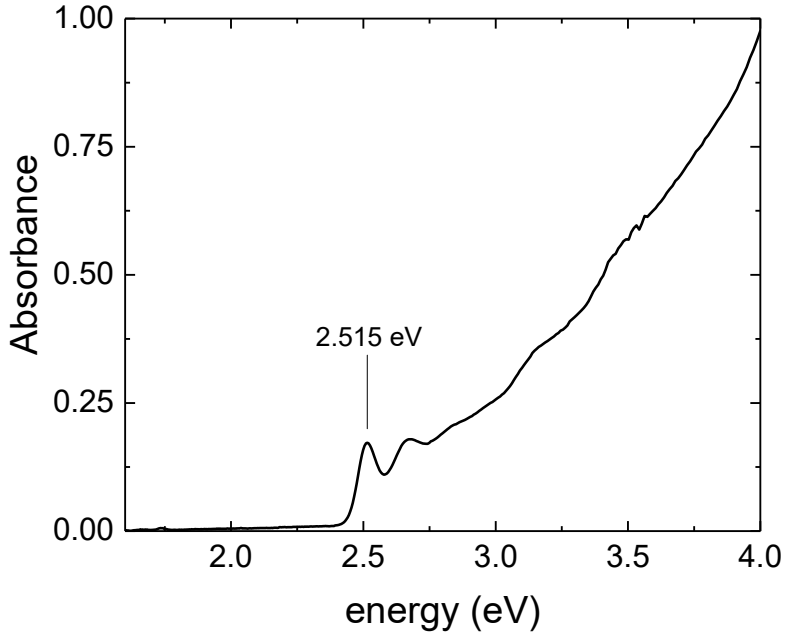

Figure S1. The optical absorption spectrum of as-synthesized ~8 nm $CsPbBr_3$ nanocrystals dispersed in toluene.

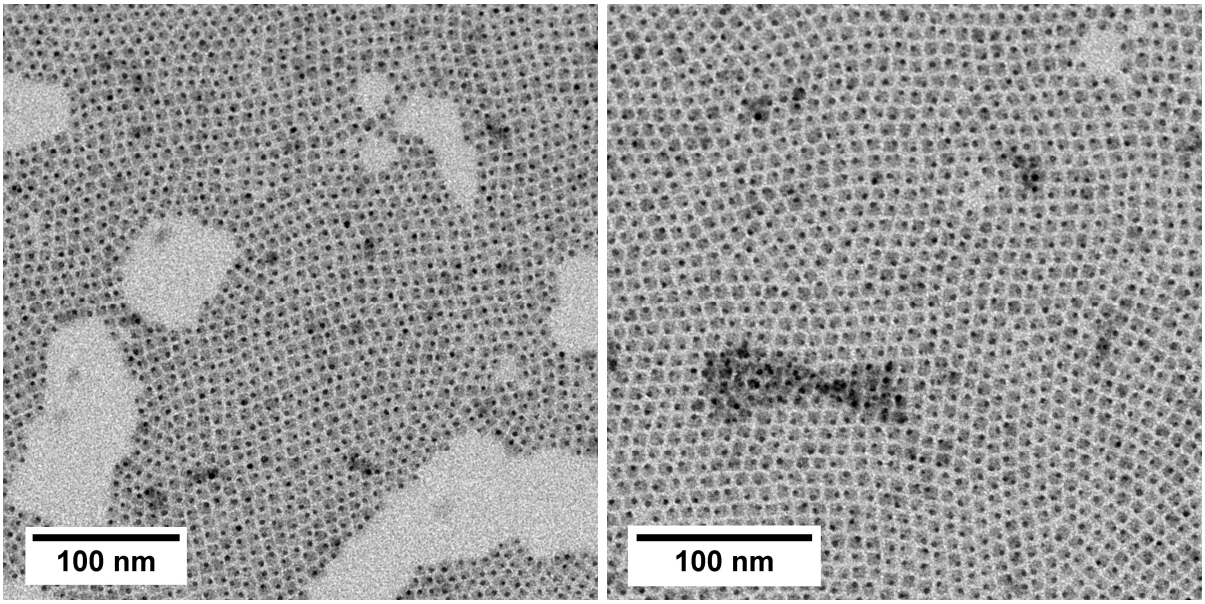

Figure S2. TEM images of as-synthesized ~8 nm $CsPbBr_3$ nanocrystals. The high contrast black dots appearing on the nanocrystals are metallic lead particles formed as a result of the electron beam damage in TEM.

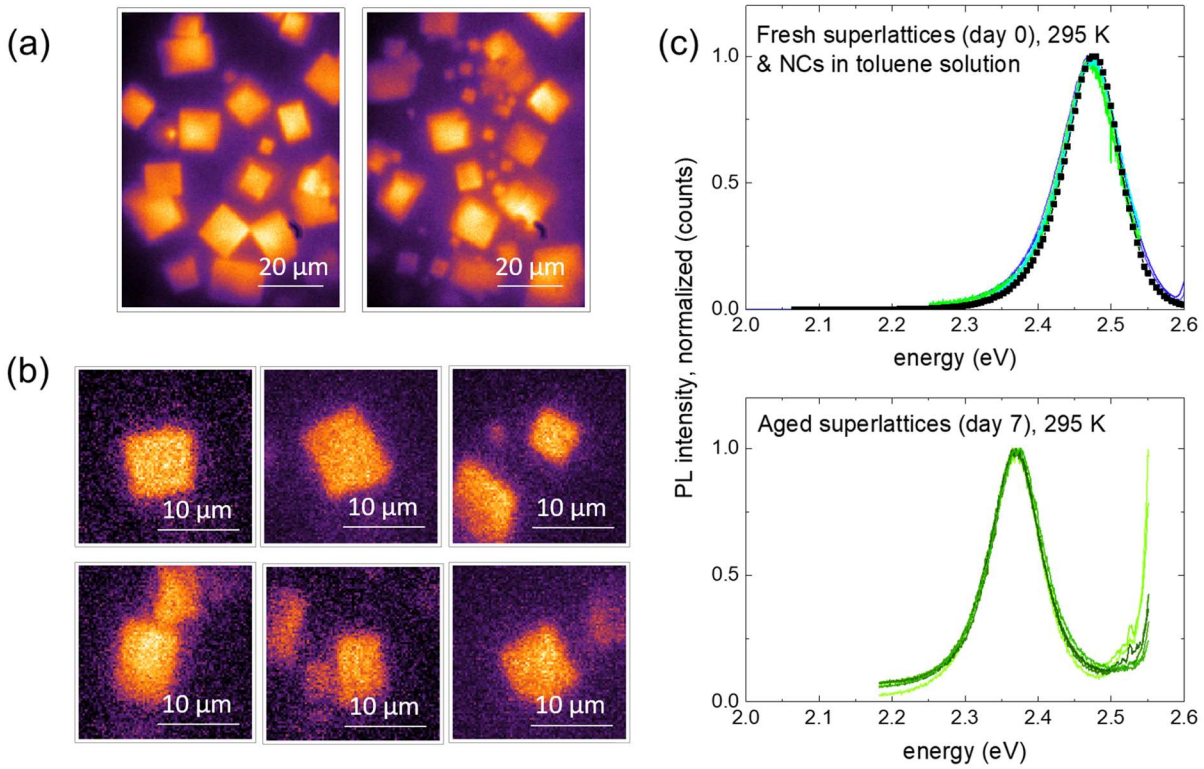

Figure S3. False-colored room temperature micro-PL images of (a) fresh $CsPbBr_3$ nanocrystal superlattices on the day of their preparation and (b) a week later (aged in vacuum) with corresponding PL spectra (c): 5 fresh superlattices (top panel, overlaid colored curves) and 7 aged superlattices (bottom panel, overlaid colored curves). The PL spectrum of a dilute toluene dispersion of starting $CsPbBr_3$ nanocrystals in toluene is also shown in (c) for comparison (top panel, black curve+black squares). The brightness of images in panels (a) and (b) corresponds to the PL intensity.

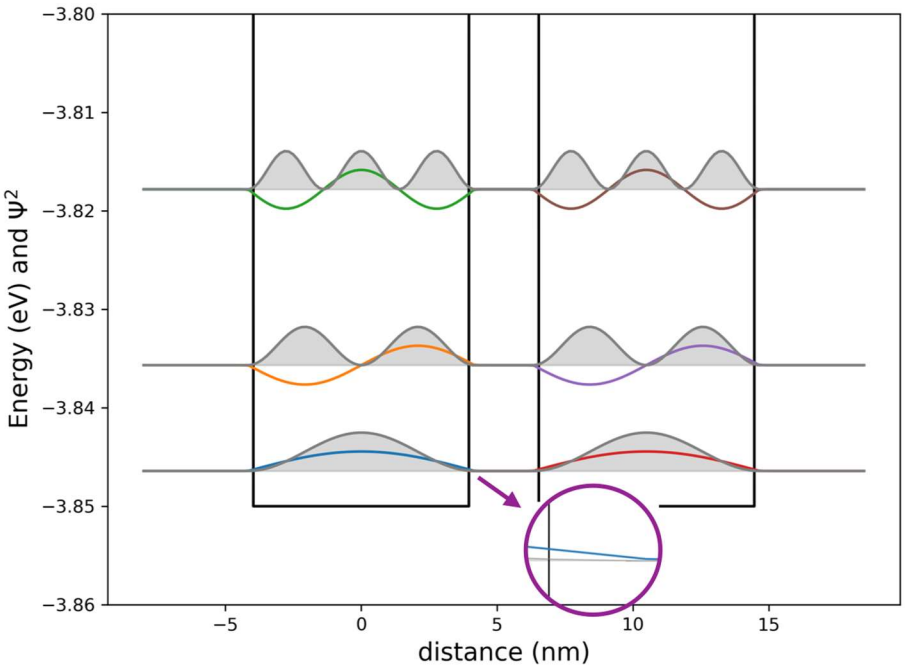

Figure S4. Wavefunctions of a free carrier in a 1D well approximating $CsPbBr_3$ nanocrystal (3.85 eV deep, 8 nm wide). The black line indicates the potential well, and the colored lines are the wavefunctions for state = 1, 2, 3, respectively. The gray area indicates the probability (Ψ^2). The schematic shows two neighboring nanocrystals with 2.5 nm separation. The inset shows the wavefunction leakage outside the well, which is significantly smaller than the crystal separation.

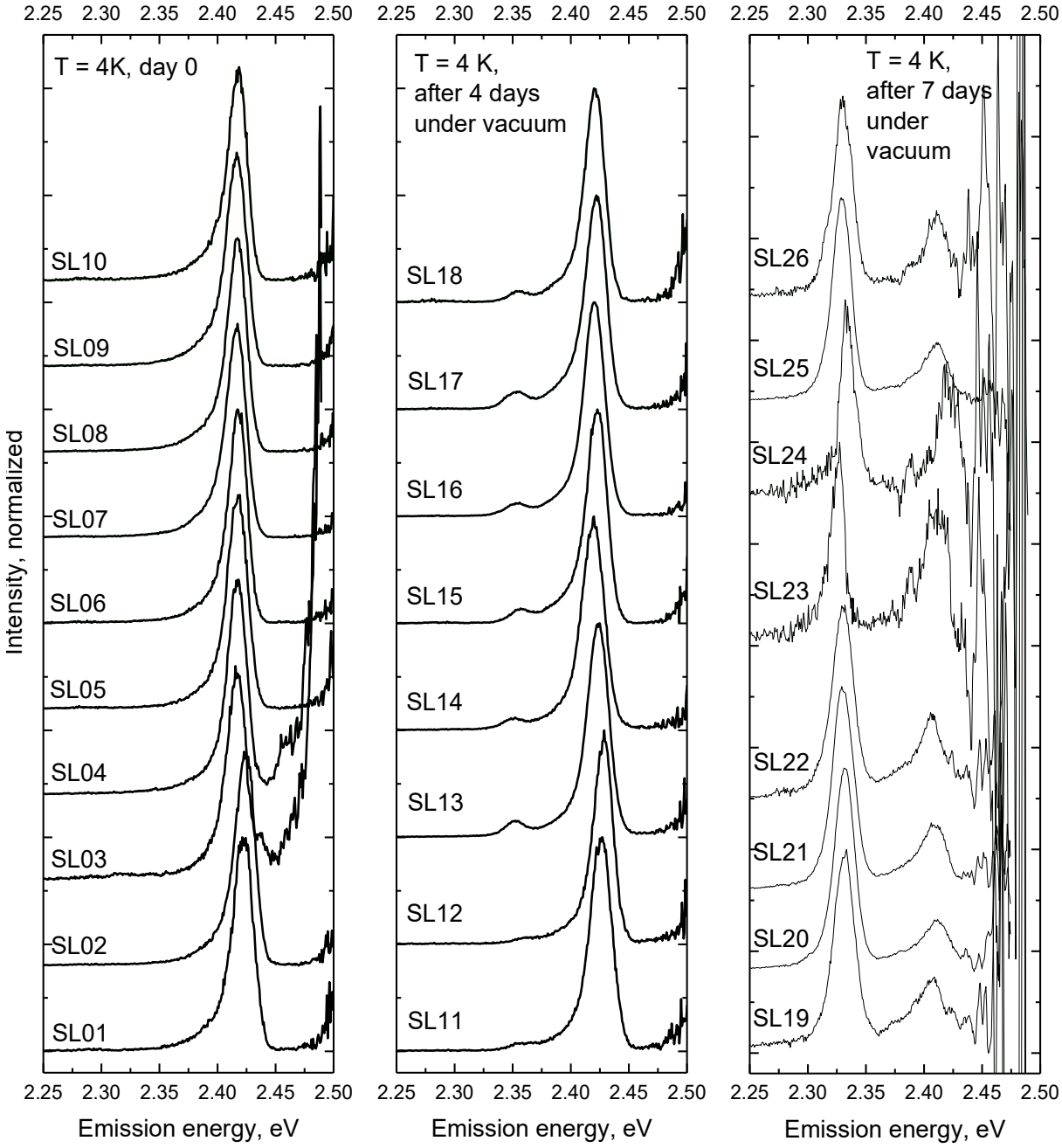

Figure S5. Cryogenic (T = 4K) micro-PL spectra of individual superlattices collected when freshly-prepared (left panel) and at two stages of aging under vacuum: after ~4 days (middle panel) and after ~7 days (right panel).

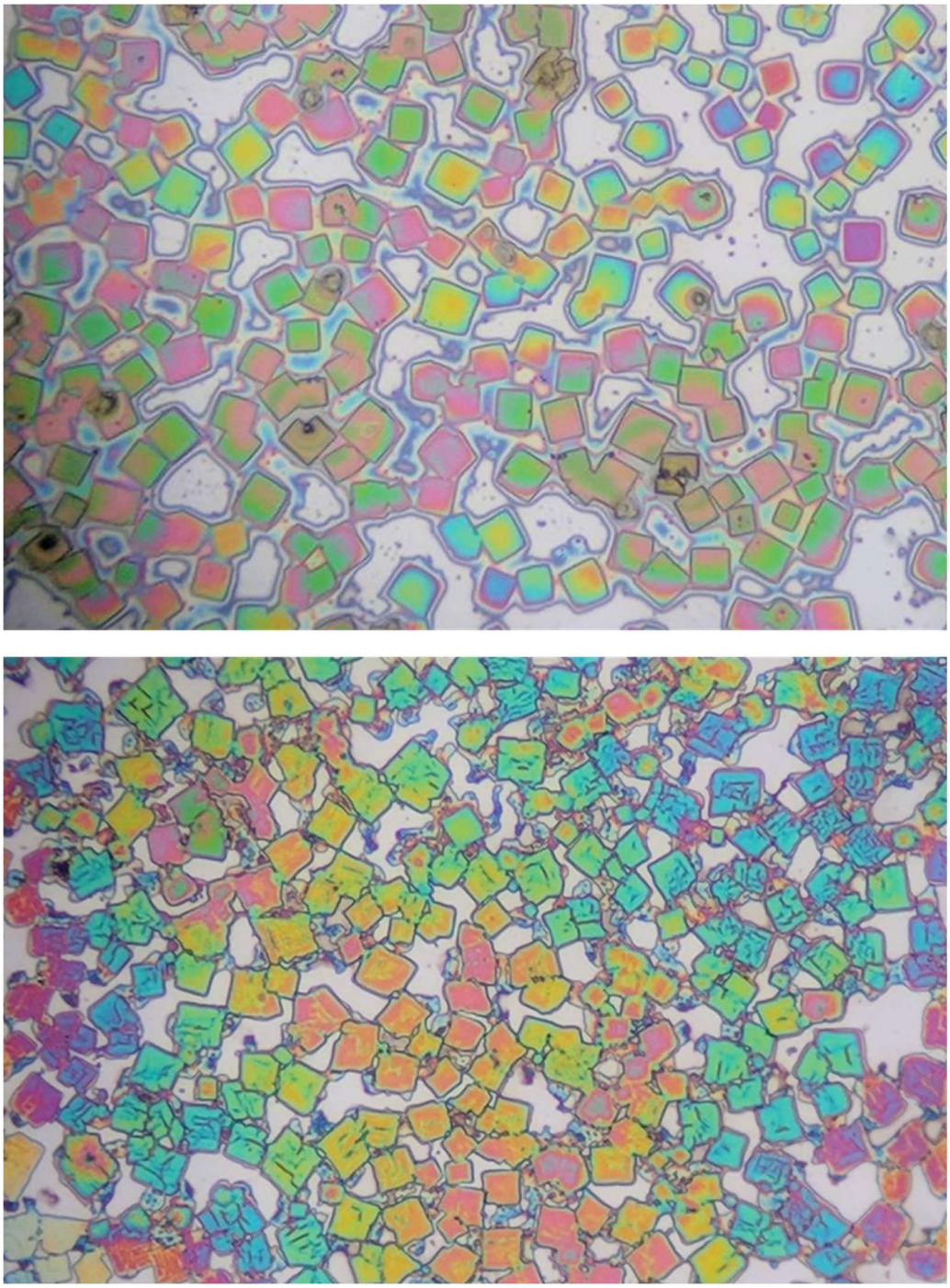

Figure S6. Optical microscopy images of another freshly-made $CsPbBr_3$ nanocrystal superlattice sample before loading into the cryostat (top image) and after the sample was kept at ~4 K under vacuum overnight (bottom image). The combination of vacuum and cooling/warming up steps resulted in superlattices being cracked and distorted. The images were acquired through one of the microscope objectives using a smartphone camera. For a sense of scale, the edge length of the biggest superlattices is ~10-20 microns (an estimate based on calibrated imaging of similar samples).

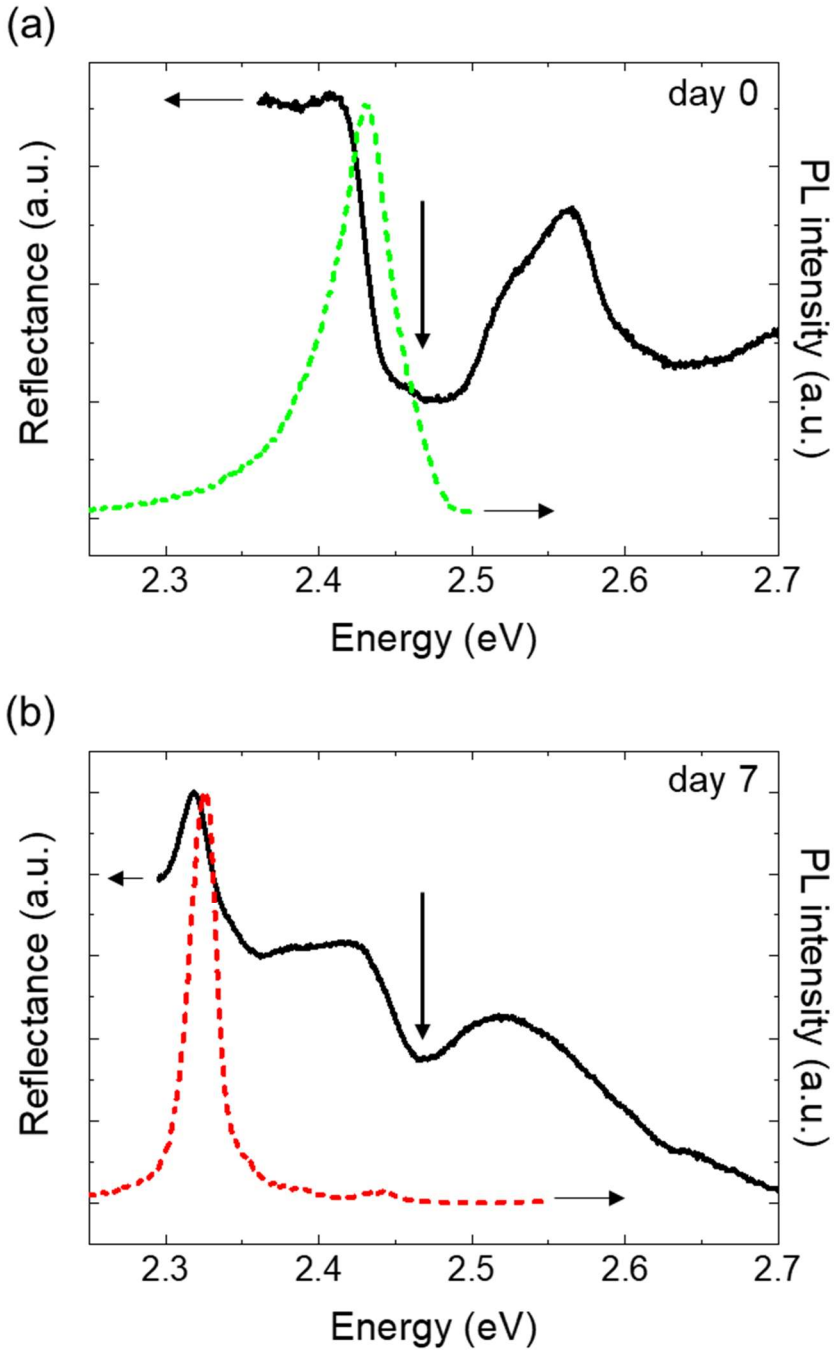

Figure S7. Reflectance (solid black curves) and PL spectra (green and red dashed curves) for (a) fresh and (b) aged (in vacuum) $CsPbBr_3$ nanocrystal superlattices measured at T = 4K. The dips in the reflectance spectra correspond to attenuation of the reflected light due to absorption, while peaks correspond to the increase in the intensity of the reflected light due to photoluminescence. The broad dips at ~2.46 eV (indicated by vertical black arrows) in the spectra are assigned to the light absorption by 8 nm $CsPbBr_3$ nanocrystals. The pronounced dip at ~2.46 eV in the reflectance spectrum of the aged superlattice confirms that it still contains a large amount of the small nanocrystals which were not fused together.

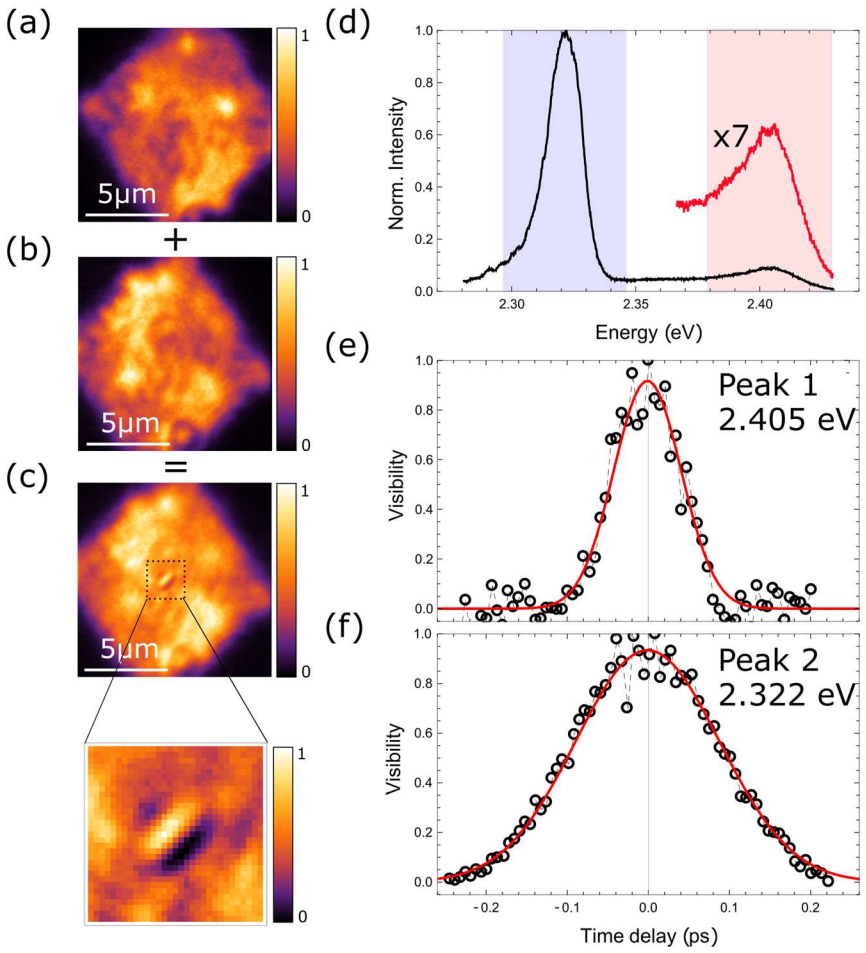

Figure S8. The first-order spatial and temporal coherence measurement of a $CsPbBr_3$ nanocrystal superlattice aged in vacuum (11 days). (a) False-colored real space micro-PL image and (b) its centrosymmetric inverted image, collected from the two arms of a Michelson interferometer. (c) False-colored real space micro-PL image obtained when the signal from the two arms is superposed at zero time delay (autocorrelation point). Brightness corresponds to the relative normalized PL intensity (a.u.) plotted on a linear scale from 0 to 1. The inset shows a zoomed-in central area of the panel (c), which highlights the formation of the interference pattern around the autocorrelation point on a scale of <1 micron. (d) PL spectrum of the investigated superlattice showing two peaks, the colored shading shows the 50 meV bandwidth of the notch filter used to separate the peaks. (e, f) Normalized time decay of the fringe visibility as a function of the time delay between the two arms of the interferometer (black circles) for the two emission peaks, high energy (peak 1, $E_{PL}^{max} \approx 2.405\ eV$) and red-shifted one (peak 2, $E_{PL}^{max} \approx 2.322\ eV$), respectively. A Gaussian function (solid red line) is used to fit the intensity decay. The estimated coherence times (1/e^2 decay time) are $\tau_{coh}^{peak\ 1} \sim 70\ fs$ and $\tau_{coh}^{peak\ 2} \sim 150\ fs$.

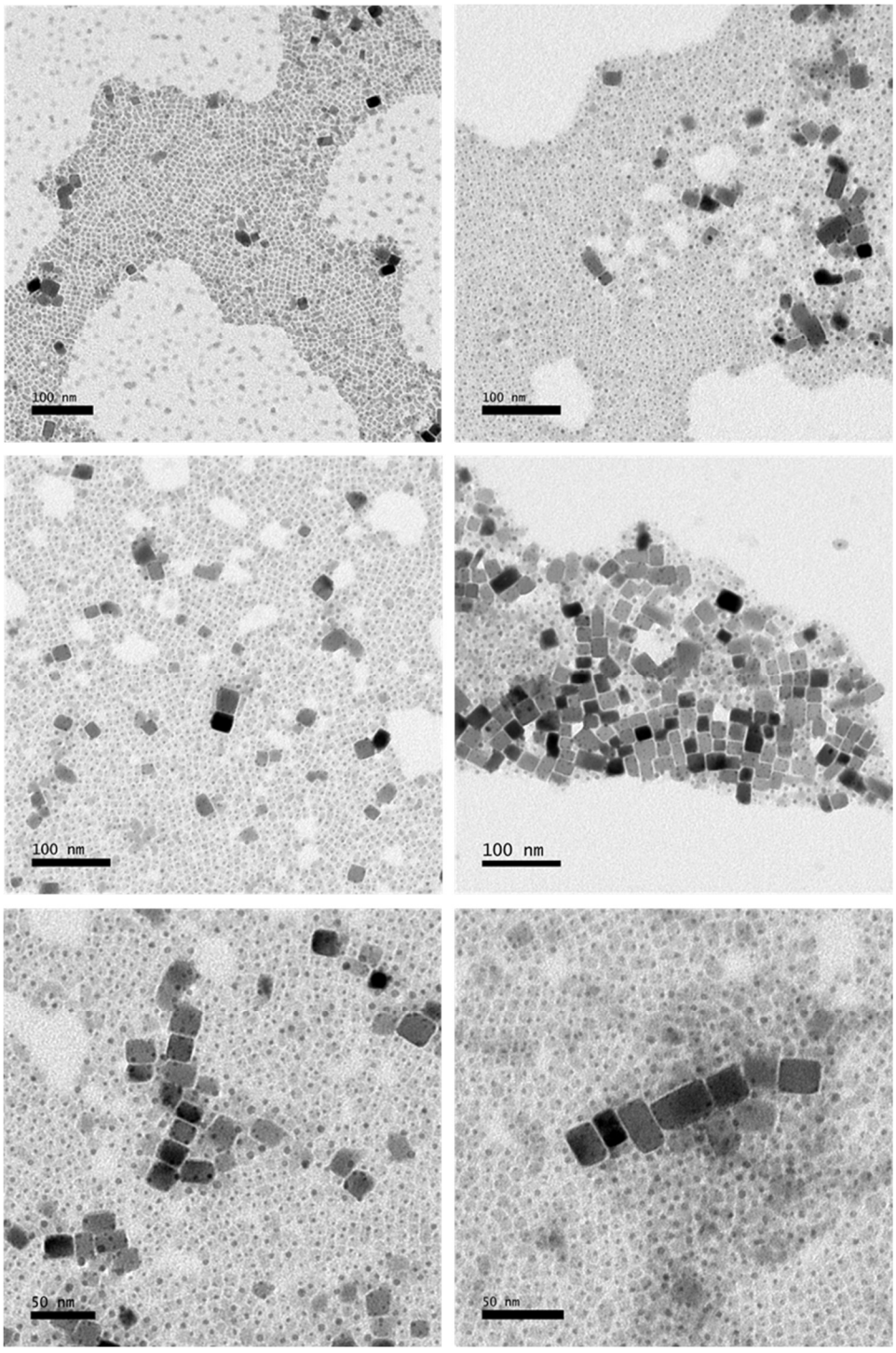

Figure S9. TEM images of the $CsPbBr_3$ nanocrystal superlattice sample aged under vacuum for ~7 days and dissolved in toluene, evidencing the presence of large $CsPbBr_3$ nanoparticles in addition to the small nanocrystals.

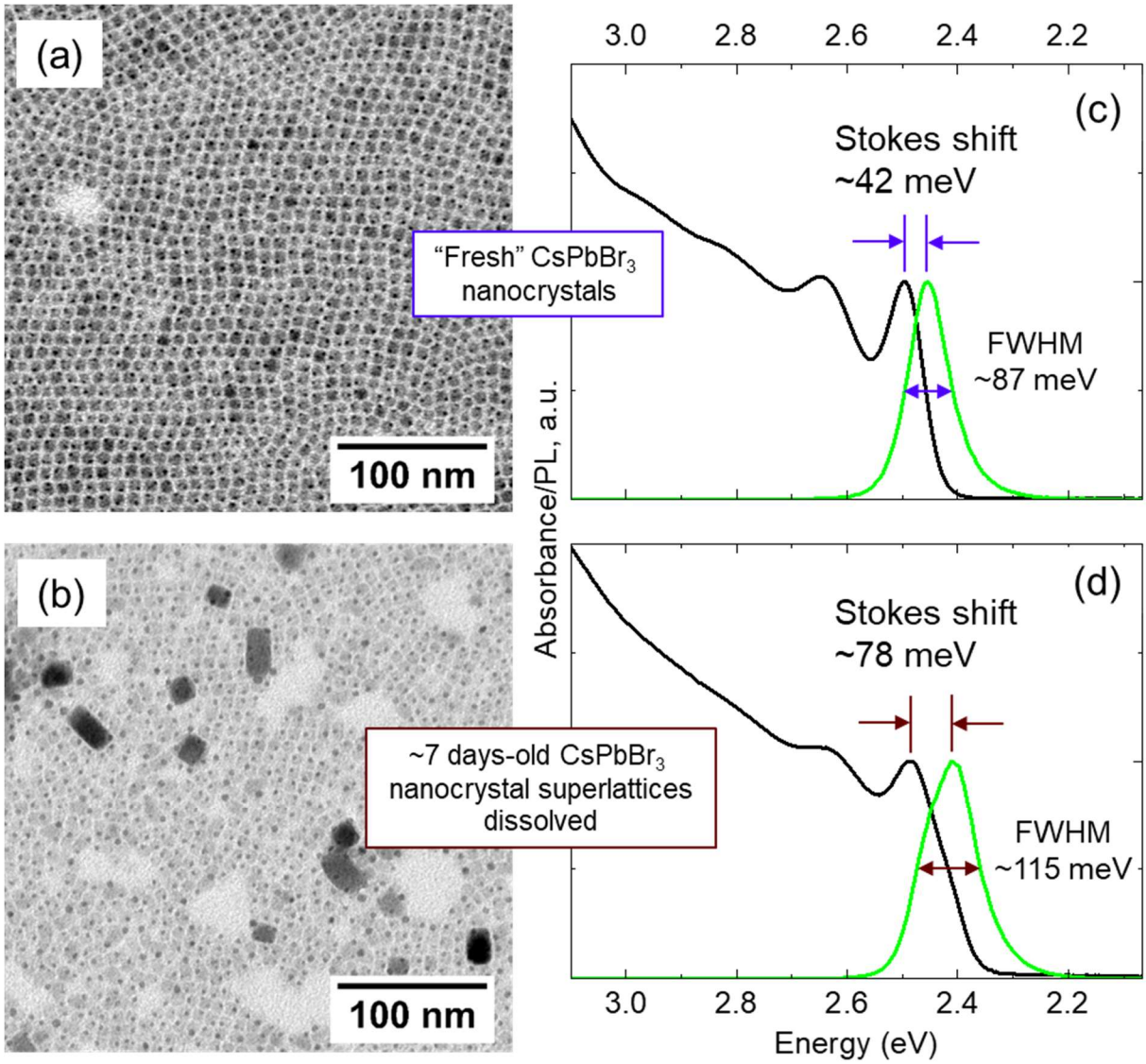

Figure S10. Comparison between TEM images, absorbance and PL spectra of dissolved fresh (a, c) and ~7 days vacuum-aged (b, d) superlattices of $CsPbBr_3$ nanocrystals. The absorption spectrum of the dissolved aged nanocrystals (d, solid black line) features broader peaks and an asymmetric low energy tail, ascribed to the combination of absorption and scattering by the larger $CsPbBr_3$ nanoparticles. PL spectrum of the aged sample (d, solid green curve) is red-shifted and broadened compared to that of the fresh sample (c, solid green line). The polydispersity of nanocrystals in the aged sample also results in a larger Stokes shift as compared to the fresh sample, as indicated by arrows in the figure.

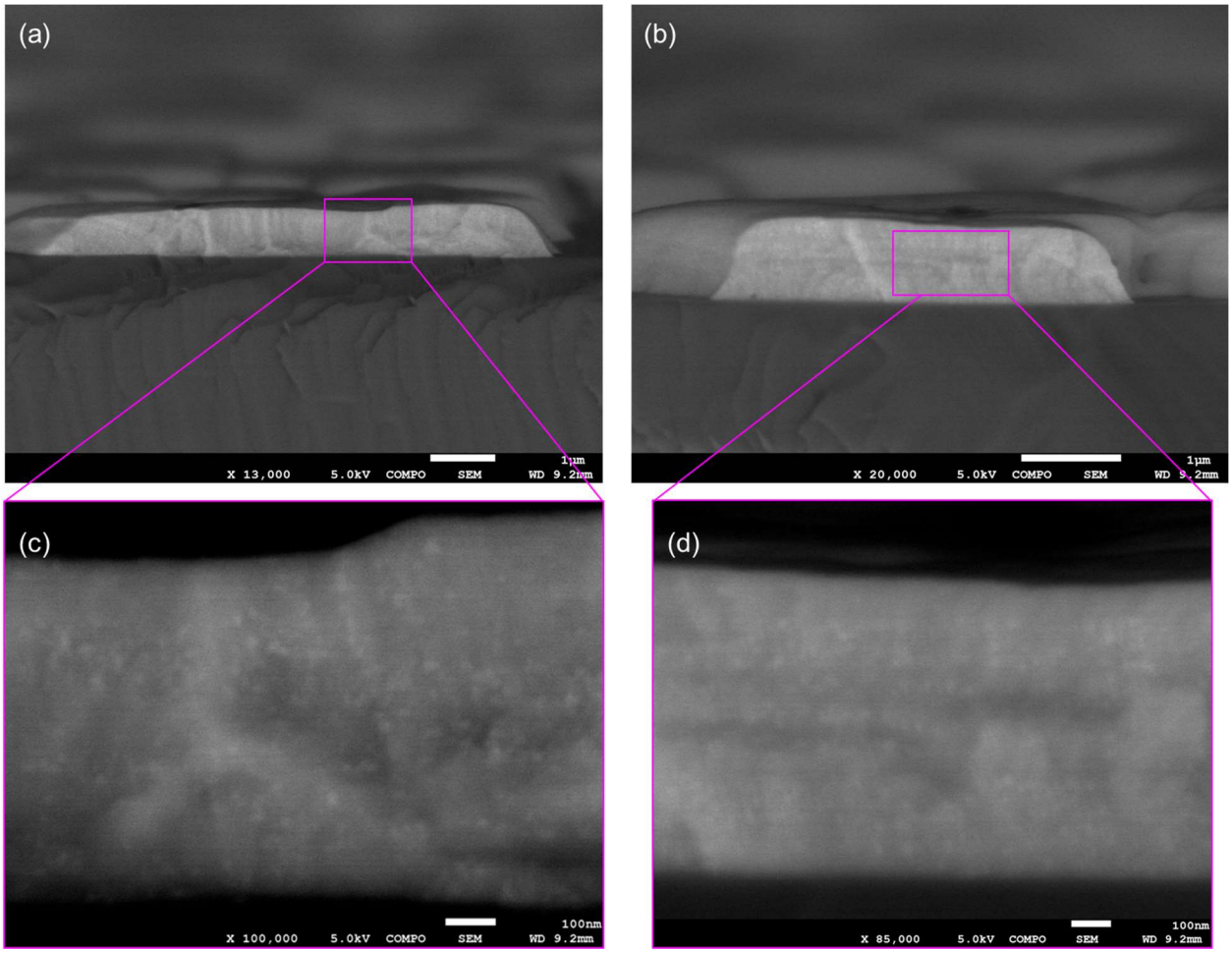

Figure S11. (a, b) Low-magnification and (c, d) high-magnification SEM images of the cross-section of $CsPbBr_3$ nanocrystal superlattice, which has been aged for ~7 days under vacuum. The scale bars are 1 micron and 100 nm in panels (a, b) and (c, d), respectively. The higher-contrast bright spots in the close-up of the cross-sections (c, d) are interpreted as large, ~20-40 nm $CsPbBr_3$ nanoparticles, consistent with the TEM images of the dissolved sample in **Figures S9** and **S10b**.

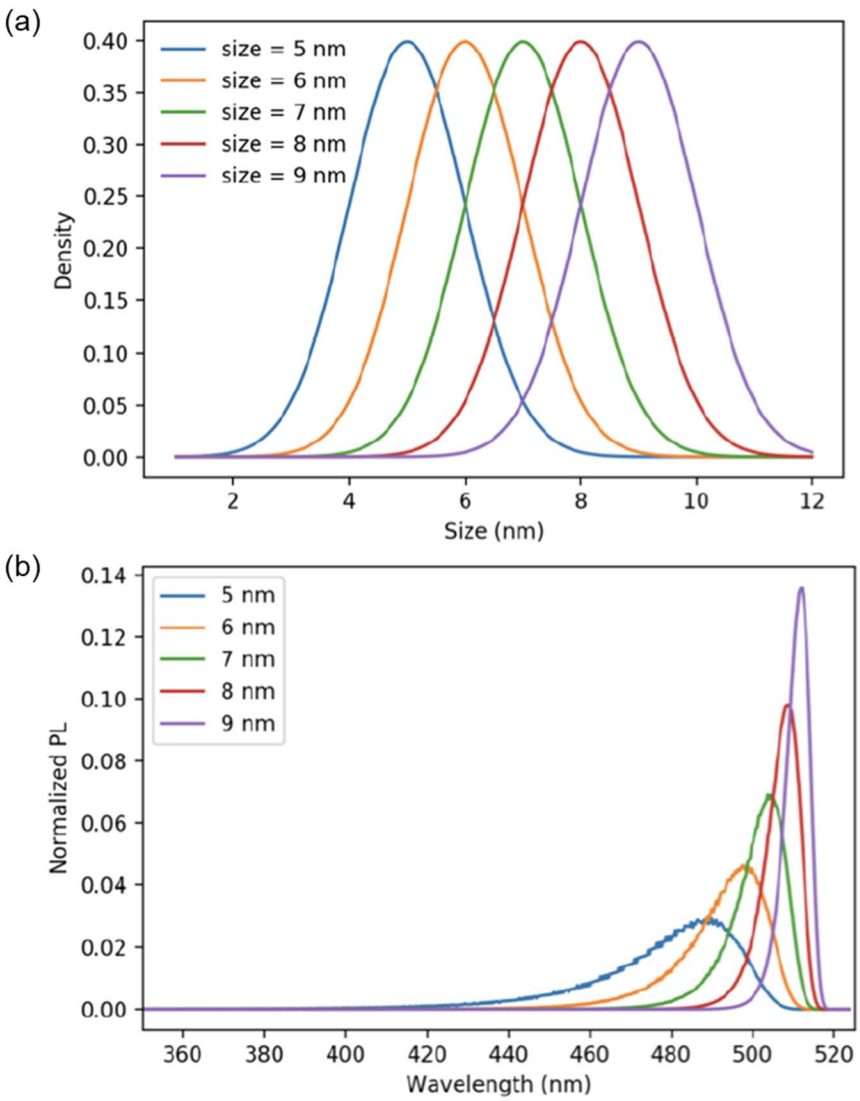

Figure S12. (a) Calculated normal size distribution for an ensemble of nanocrystals centered at 5-9 nm and a standard deviation of 1 nm. (b) Corresponding calculated area-normalized photoluminescence spectra.

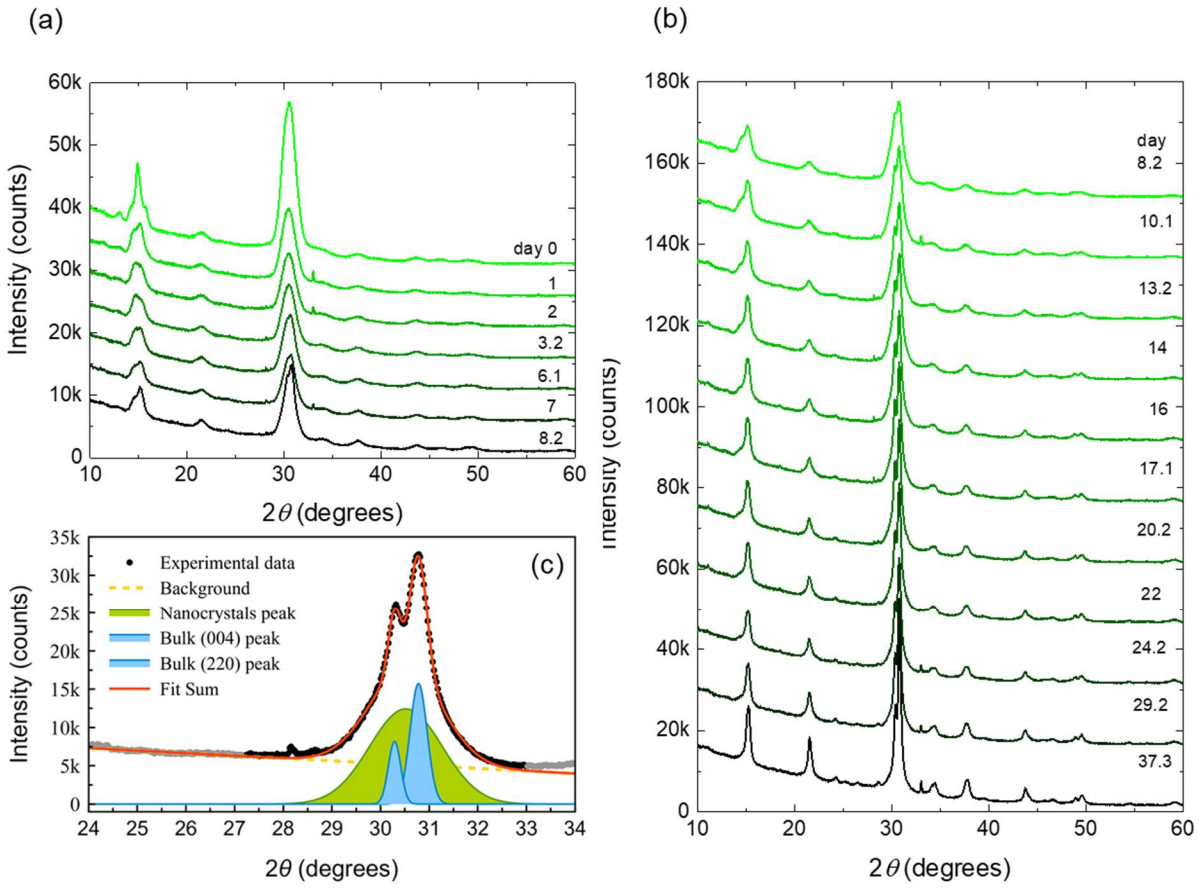

Figure S13. XRD patterns of a sample of $CsPbBr_3$ nanocrystal superlattices collected for over a month. (a) XRD patterns collected for the period of first ~8 days. (b) XRD patterns collected for the remaining period of ~8-38 days. (c) an illustration of the XRD pattern decomposition into nano and bulk contributions for a 14 day-old superlattice sample.

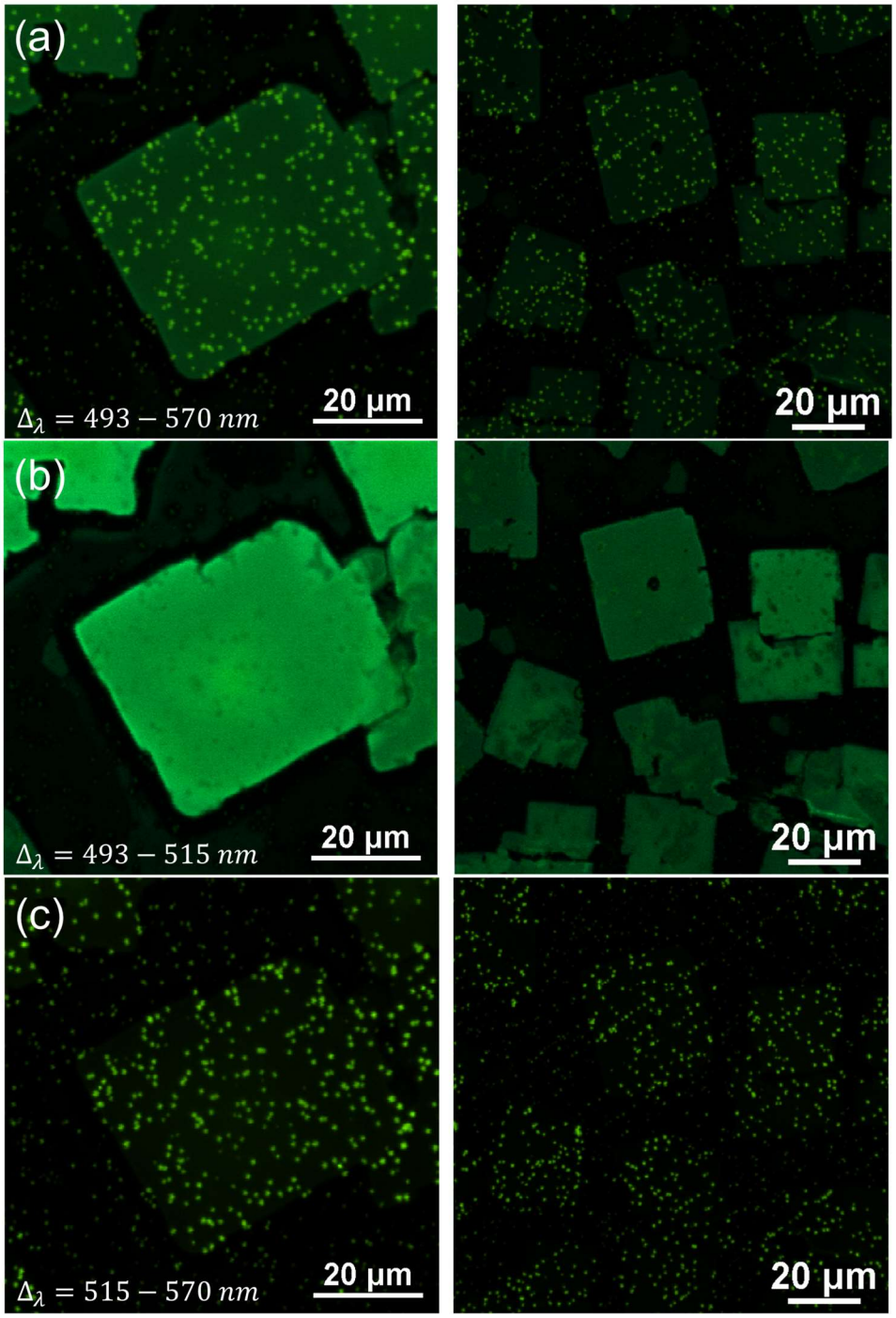

Figure S14. $CsPbBr_3$ nanocrystal superlattices aged for ~8 days in air at room temperature produce large $CsPbBr_3$ particles with a red-shifted PL spectrum, as can be detected by the micro-PL inspection. Two columns show spectrally resolved images from two areas of the same sample. Row (a) shows a PL intensity distribution across the entire detected spectral range of 493-570 nm. Rows (b) and (c) show PL intensity distribution over high energy (493-515 nm) and low energy (515-570 nm) spectral regions, respectively.

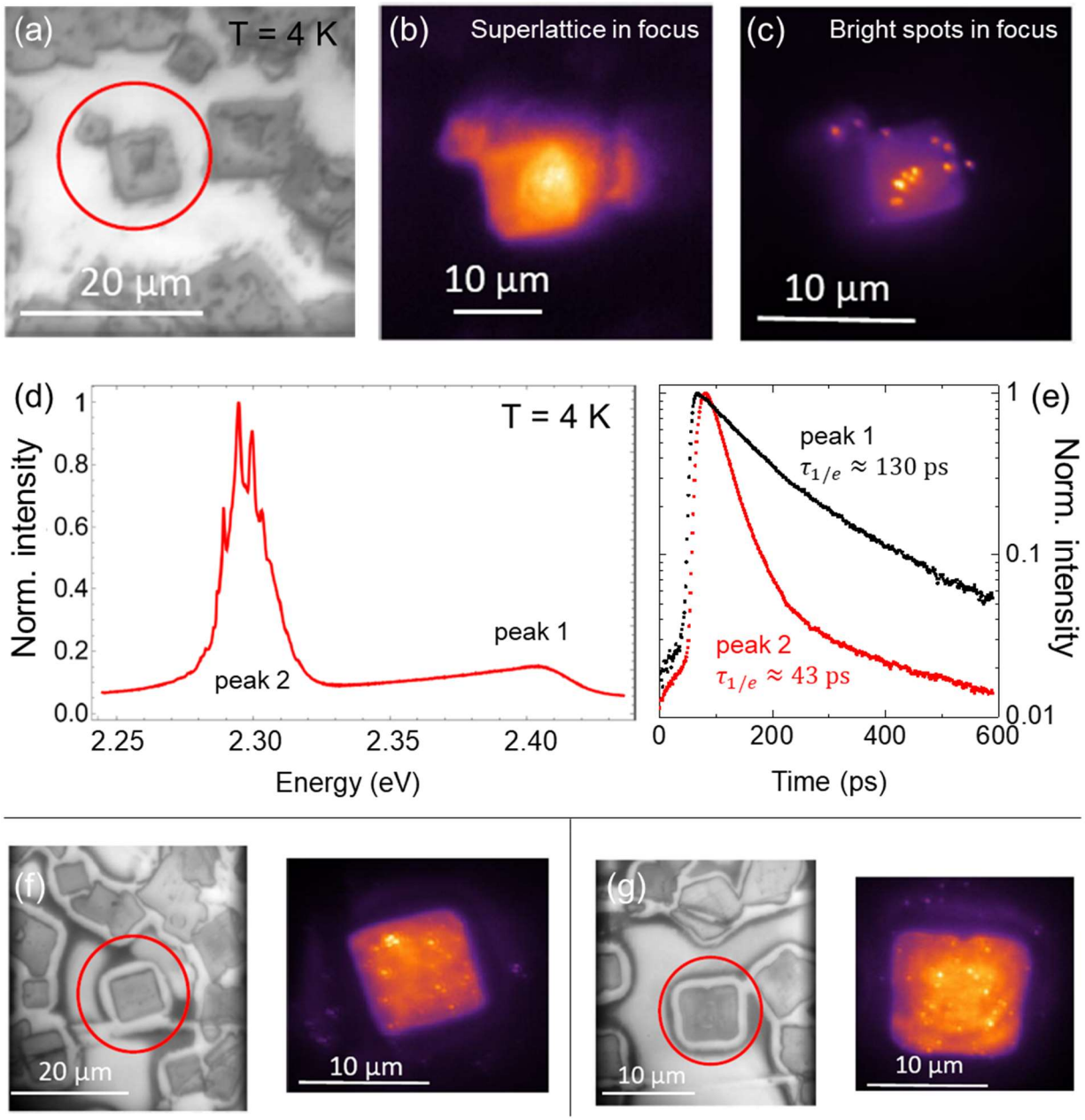

Figure S15. Additional cryogenic (T = 4K) micro-PL data for $CsPbBr_3$ nanocrystal superlattices aged in air. (a) white light intensity reflectance image of a selected superlattice (highlighted by a red circle); false-colored micro-PL images of the superlattice with a focus on (b) the body of the superlattice and (c) on the bright spots; (d) steady-state PL spectrum of the superlattice showing two peaks; (e) time-resolved PL intensity decays for each of the peaks; (f) and (g) show two other examples of the superlattices in reflectance (left image) and false-colored micro-PL (right image).

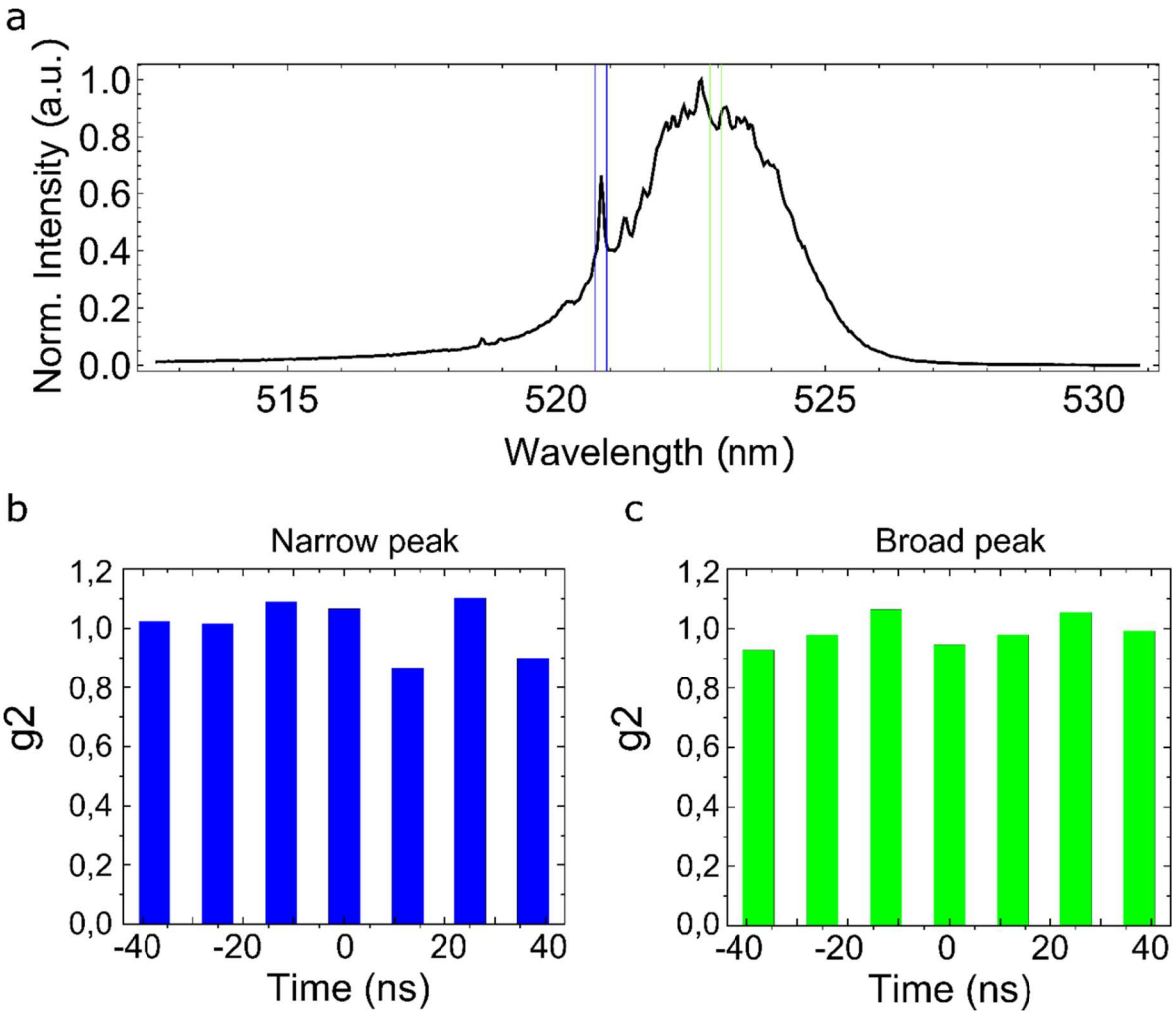

Figure S16. (a) T = 4 K emission spectra of a $CsPbBr_3$ nanocrystal superlattice sample grown on glass and aged in air for one week, showing the red-shifted emission with narrow peaks. The energy of the aged PL is higher than for the samples discussed in the main text, possibly due to the uncontrolled factors affecting aging of $CsPbBr_3$ nanocrystal superlattices in air. (b-c) $g^{(2)}(\tau)$ experiments performed on the narrow peak (b) and the broad emission peak (c) after spectrally resolving the photoluminescence using a spectrometer with a selected spectral region of 0.2 nm showing that no bunching is occurred.

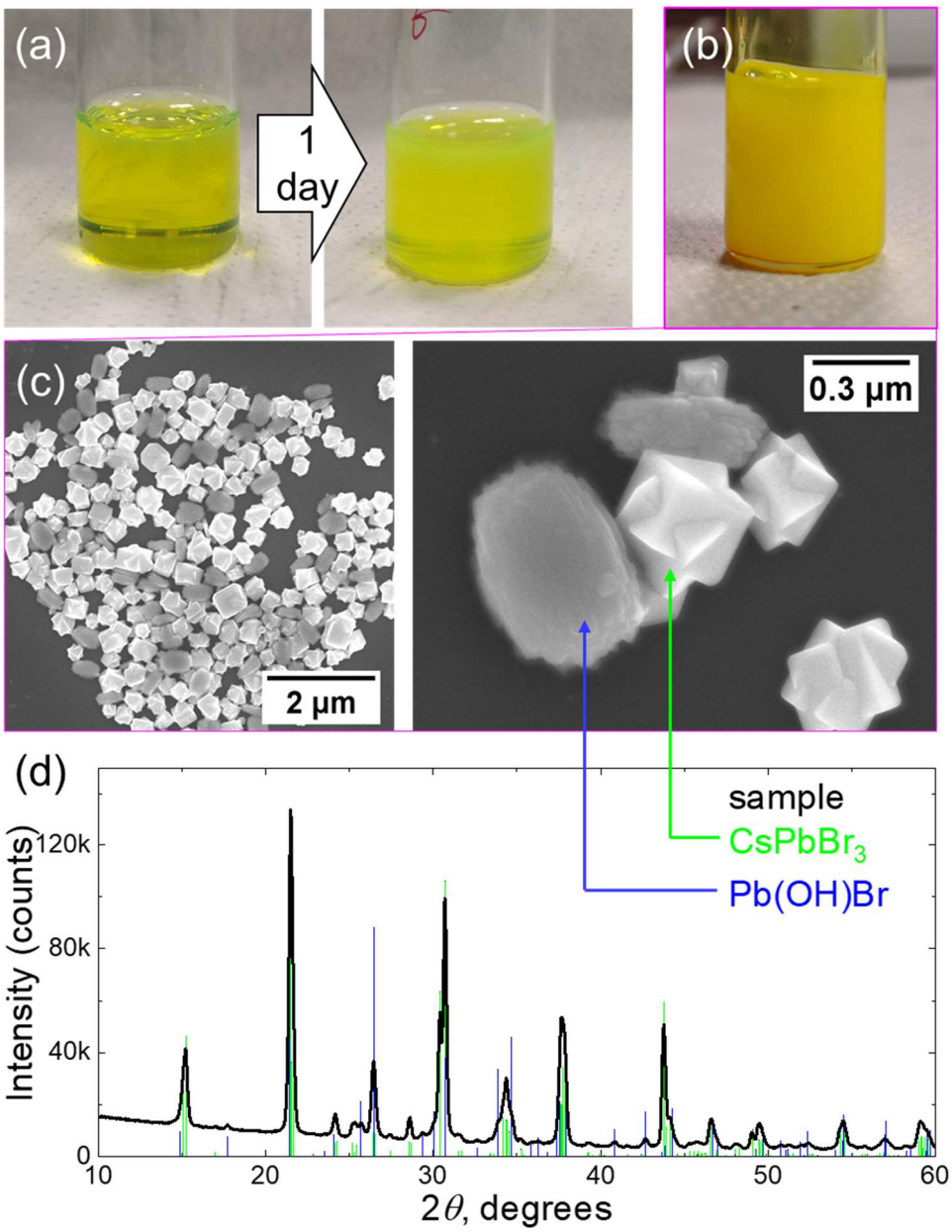

Figure S17. (a) An initially transparent, luminescent green under room lights, solution of $CsPbBr_3$ nanocrystals turns cloudy within a day of storage in air. (b) Concentrated, ~7 days old sample of $CsPbBr_3$ nanocrystals has lost the original luminescent glow and turned into a cloudy yellow suspension. (c) Low-and high-magnification SEM images of the precipitate isolated from the sample shown in (b) by centrifugation, showing two populations of particles – high contrast faceted ones (composition $Cs_1Pb_{1.37}Br_{2.89}$ by single-particle EDS) and lower contrast ellipsoidal ones ($Cs_{0.03}Pb_1Br_{1.07}$). (d) XRD pattern of the precipitate imaged in (c). The compounds identified by XRD are orthorhombic $CsPbBr_3$ (COD code 4510745,[1] green stick reference pattern) and laurionite-type Pb(OH)Br (ICSD ref. code 404573,[2] blue stick reference pattern). Thus, Cs-poor, low contrast ellipsoidal particles are assigned the Pb(OH)Br composition, while high contrast faceted particles are assigned the $CsPbBr_3$ composition.

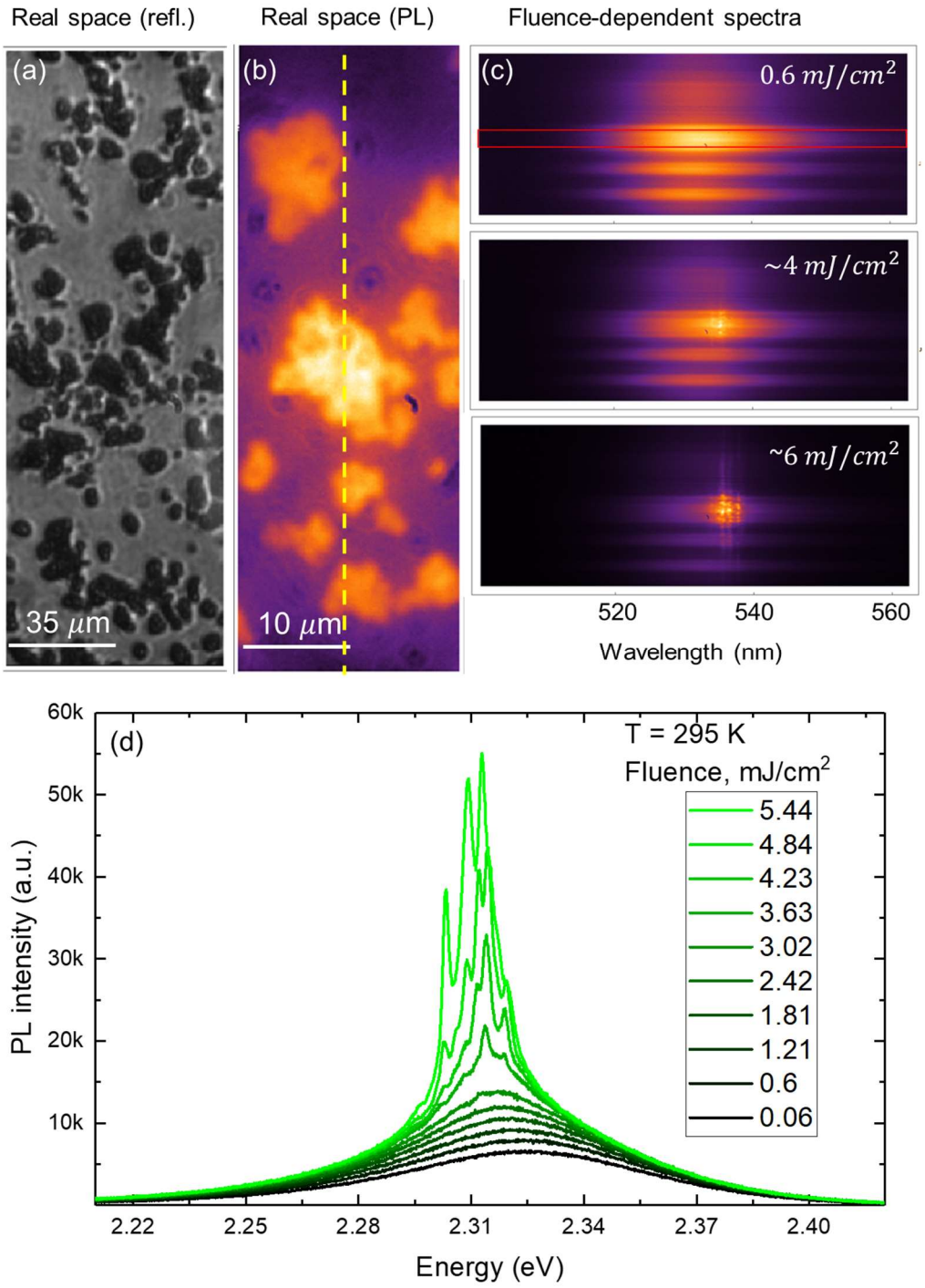

Figure S18. Excitation fluence-dependent micro-PL of the sample of bulk-like $CsPbBr_3$ particles at room temperature. (a) Real space reflectance image with white light, (b) PL from a zoomed-in region in the real space under the lowest excitation fluence of ~60 μJ/cm^2 (470 nm pulsed laser), (c) spectral images taken under increasing fluence along the region in space indicated by a dashed yellow line in panel b, red box shows a region of interest for the integrated spectra, (d) integrated PL spectra as a function of excitation fluence.

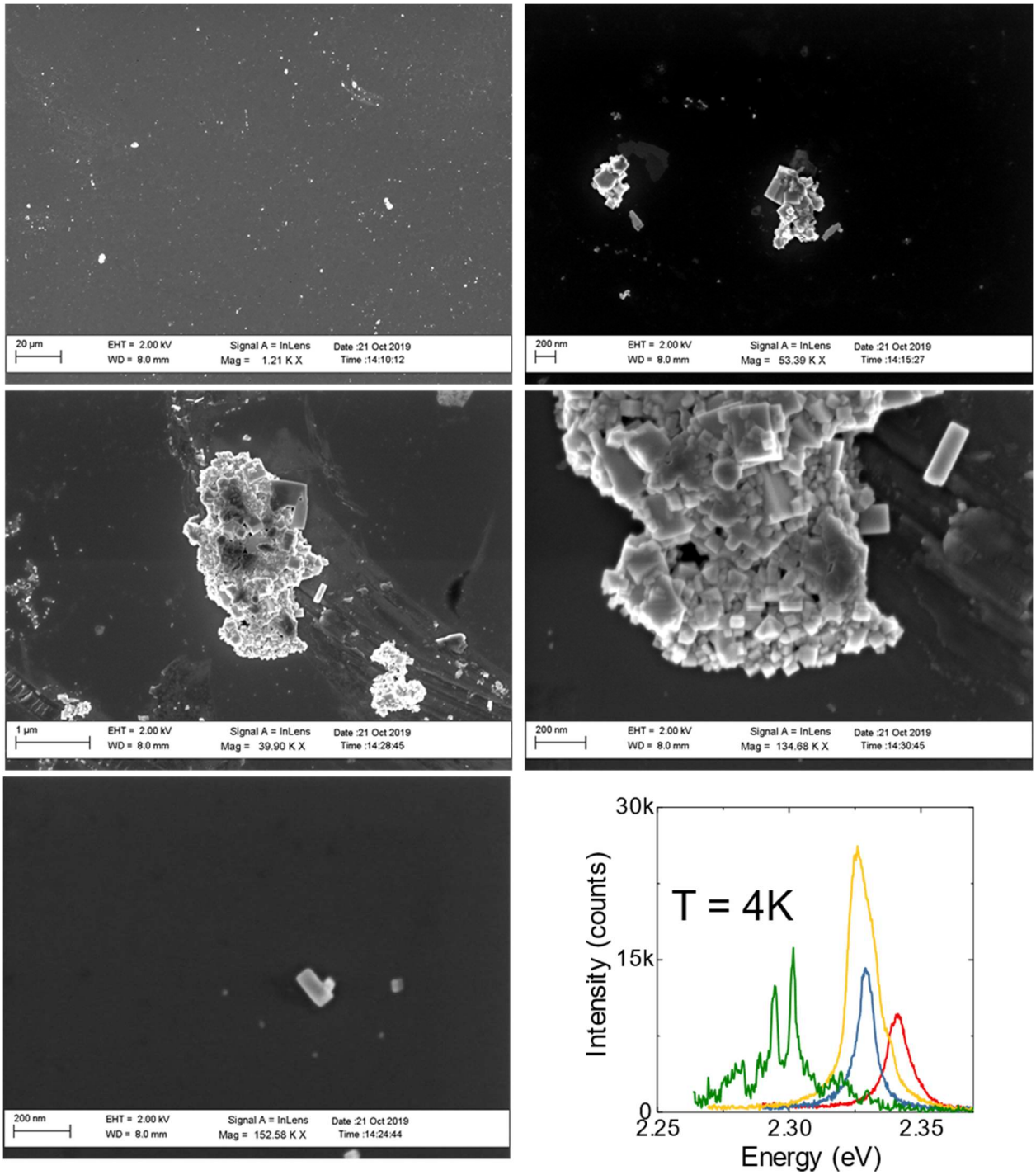

Figure S19. SEM images of the sample of bulk-like $CsPbBr_3$ particles sparsely covering Si wafer, which was studied with micro-PL spectroscopy at 4K. The distribution of particles varies from aggregates to isolated particles. In micro-PL, all these structures appear as bright spots. The differences between optical properties such as steady-state PL spectra (lower right panel) of different regions in the same sample are interpreted as coming from various morphologies, shapes, and degrees of clustering between bulk-like $CsPbBr_3$ particles.

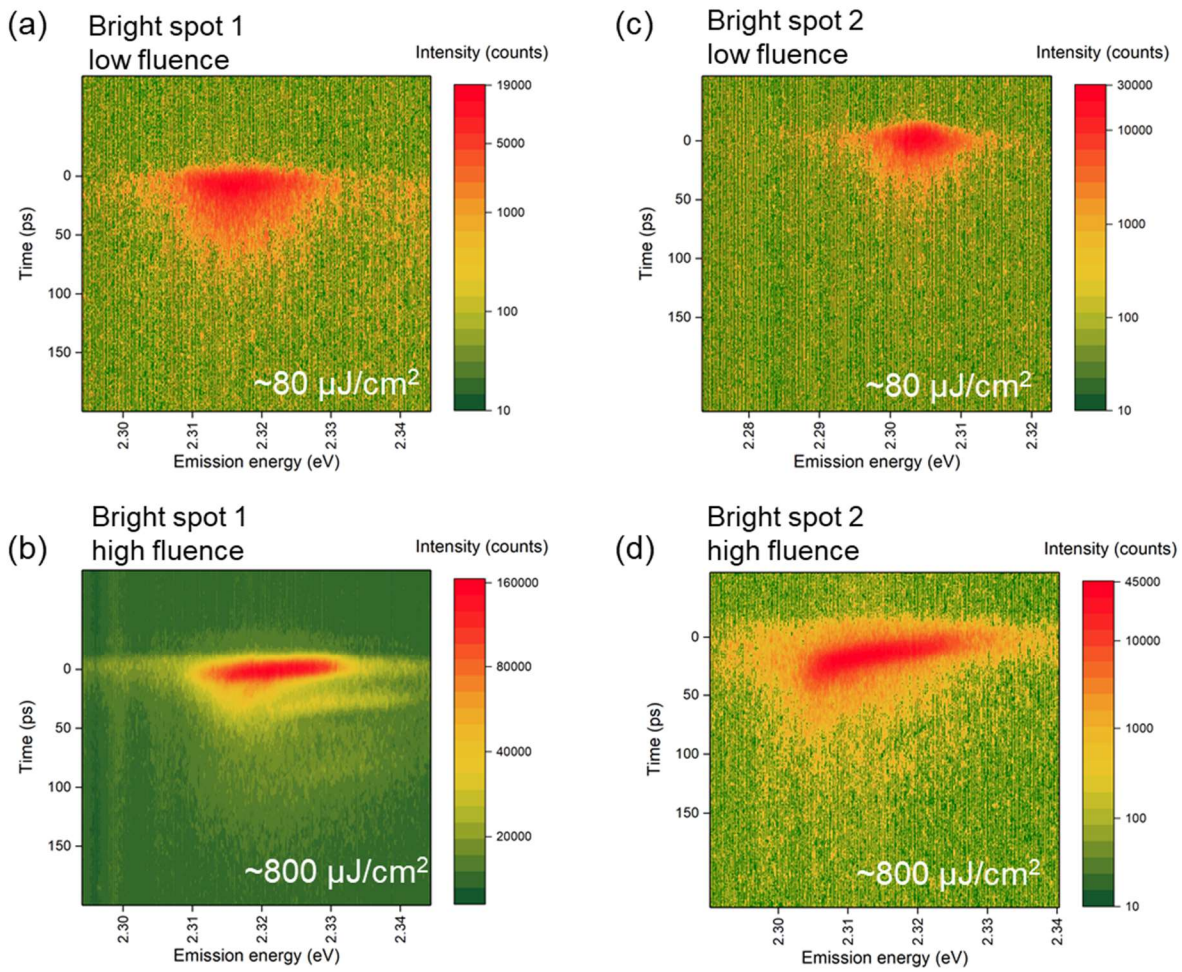

Figure S20. Streak camera images of the PL intensity decays at T = 4 K from two additional regions in the sample of bulk-like $CsPbBr_3$ particles collected at low (a, c) and high (b, d) excitation fluences ($\lambda_{exc} = 470\ nm$ and 10 kHz repetition rate, fluences ~80 and ~800 μJ/cm^2, respectively). The oscillatory decay is visible in panel (b), while the filament-shape of the temporal PL intensity decay profile is apparent in (d).

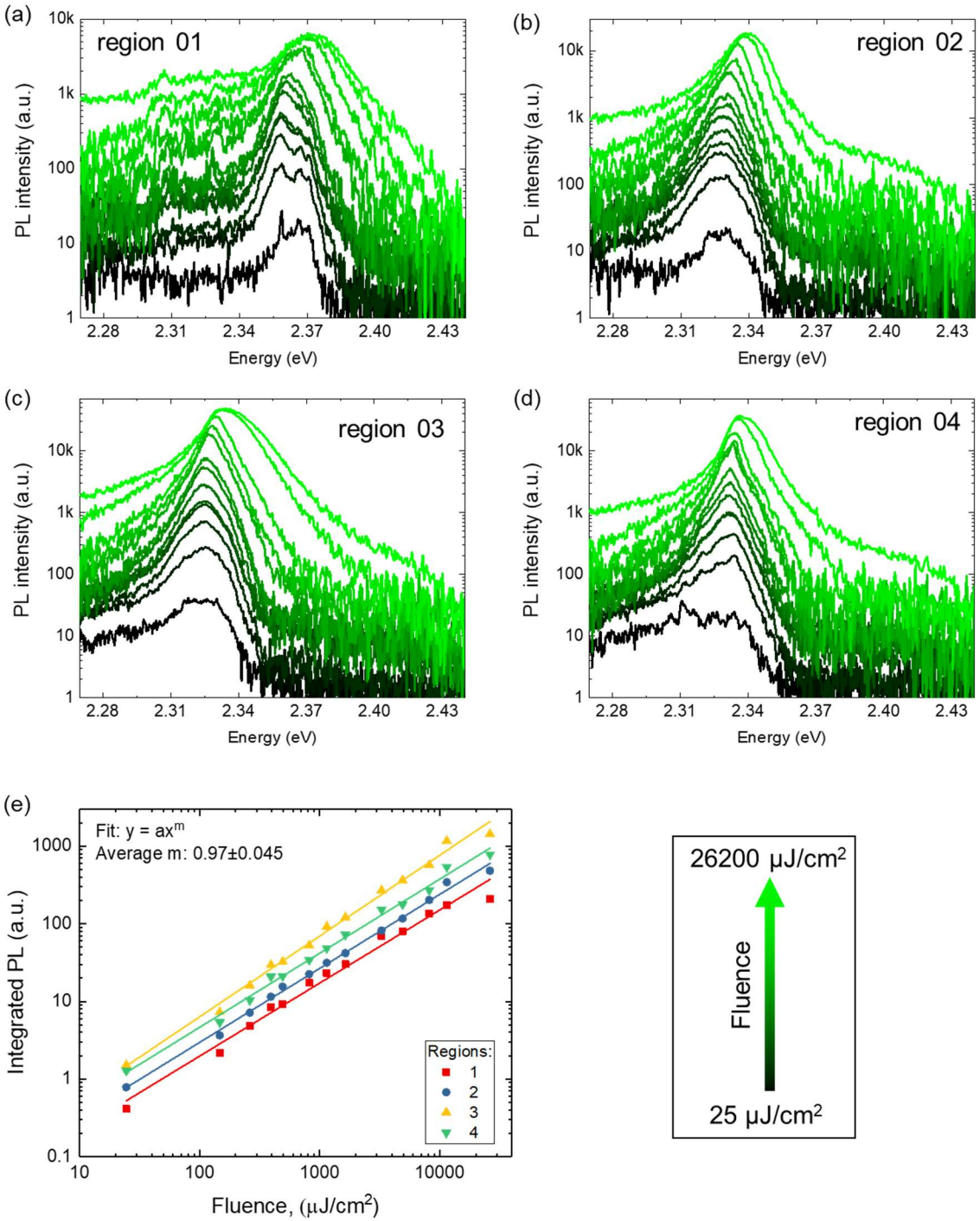

Figure S21. (a-d) Excitation fluence-dependent spectra of four regions in the sample of bulk-like $CsPbBr_3$ particles at T = 4K. The estimated fluence values are color-coded from black to green (470 nm pulsed laser, $\mu J/cm^2$): ~25, 148, 262, 394, 492, 820, 1148, 1640, 3280, 4920, 8200, 11480, 26240. (e) Integrated PL intensity dependence for the same regions. The data were fit to a power law ($y = ax^m$), with an average exponent of 0.97±0.045.

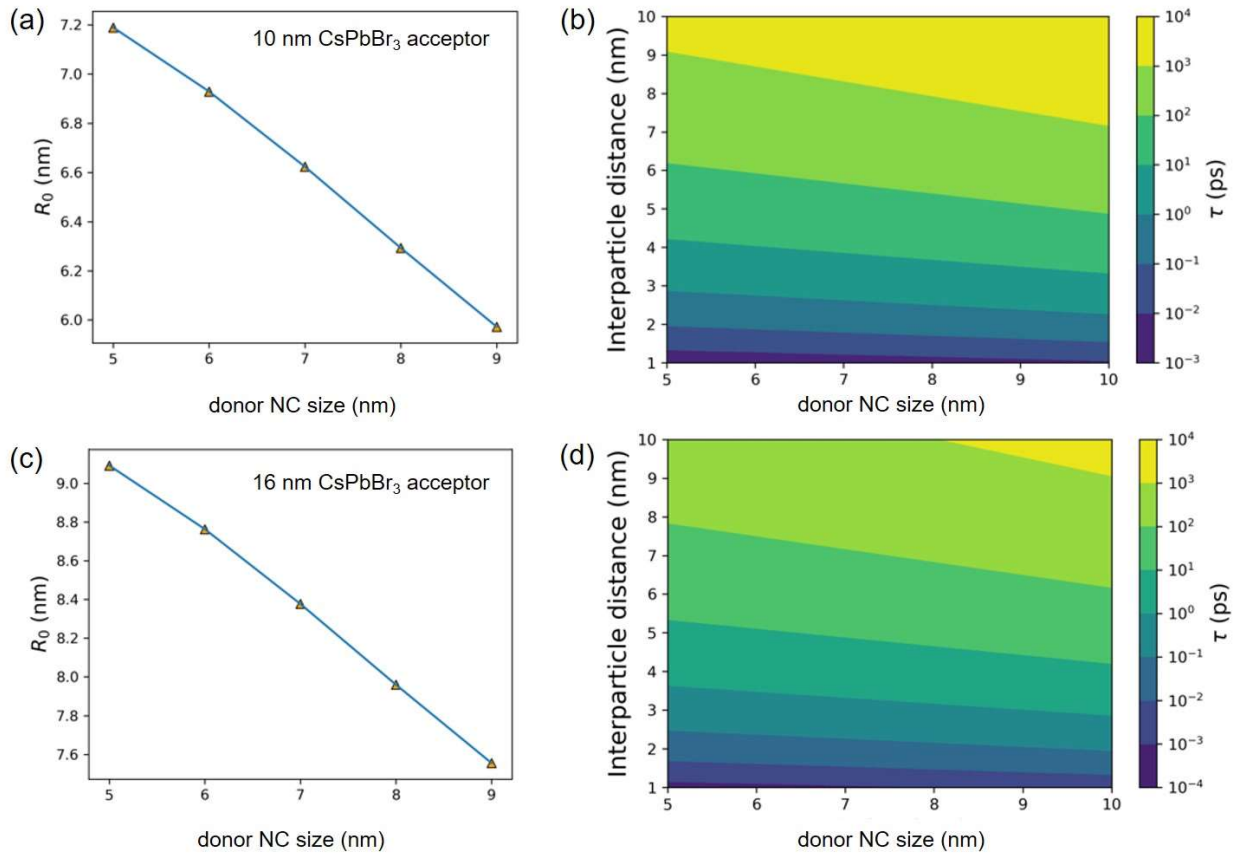

Figure S22. Calculated R_0 (a, c) and FRET rate (b, d) for 10 nm and 16 nm $CsPbBr_3$ acceptor nanocrystals, respectively. For 10 nm acceptor, the results are very similar to the 12 nm case, where τ ranges from 10^{-3} to 10^4 ps. For 16 nm acceptor, the FRET radius R_0 has increased by 1-2 nm, resulting in slightly reduced FRET rates.

Table S1. Energy-resolved PL intensity decay fit parameters for the fresh sample at T = 4 K (**Figure 6b**), amplitude-weighted average lifetime was calculated as $\langle\tau\rangle = (\sum A_i\tau_i)/\sum A_i$. The error bars indicate 95% confidence intervals as calculated by nonlinear fit in Origin 2017 software, ver. 94E.

Energy band center (5 meV width)	τ_1, ps * = fixed	A_1, counts	τ_2, ps	A_2, counts	$\langle\tau\rangle$, ps	A_1:A_2 ratio
2393	251±1.4	20058±116	-	-	251±1.4	1:0
2398	248±1.2	25569±132	-	-	248±1.2	1:0
2403	*250	28127±433	113±14	5764±406	227±5.8	0.83:0.17
2408	*250	31250±642	128±8.4	12044±483	216±6.1	0.72:0.28
2413	*250	34385±918	141±6.2	20091±690	210±6.8	0.63:0.37
2418	*250	29464±825	138±3.1	38652±614	187±4.7	0.43:0.57
2423	*250	17692±519	125±1.7	55212±441	155±2.7	0.24:0.76
2428	*250	12557±257	101±1.1	56646±509	128±1.8	0.18:0.82
2433	*250	9761±153	81±1	52537±687	108±1.8	0.16:0.84
2438	*250	7705±110	70±1	43728±782	97±2.1	0.15:0.85

Table S2. Energy-resolved PL intensity decay fit parameters for the aged sample at T = 4 K (**Figure 6d**), amplitude-weighted average lifetime was calculated as $\langle\tau\rangle = (\sum A_i\tau_i)/\sum A_i$. The error bars indicate 95% confidence intervals as extracted from a nonlinear fit in Origin 2017 software, ver. 94E.

Energy band center (10 meV width)	τ_1 (slow), ps * = fixed	A_1, counts	τ_2 (fast), ps	A_2, counts	$\langle\tau\rangle$, ps	A_1:A_2 ratio
2295	217±1.3	6453±30	-	-	217±1.3	1:0
2305	179±1	23627±109	-	-	179±1	1:0
2315	174±0.5	22585±65	-	-	174±0.5	1:0
2325	*217	4112±51	93±1.7	4799±48	150±2	0.46:0.54
2405	*250	736±20	96±4.7	764±21	172±5.4	0.49:0.51
2415	*250	862±57	133±5.5	1268±44	180±10	0.4:0.6
2425	*250	583±33	111±2.1	2599±27	136±3.7	0.18:0.82
2435	*250	332±14	73±1.4	2958±54	91±2.6	0.1:0.9
2445	*250	195±9	52±1.7	2270±99	68±3.9	0.08:0.92

S2. References

1. Stoumpos, C. C.; Malliakas, C. D.; Peters, J. A.; Liu, Z.; Sebastian, M.; Im, J.; Chasapis, T. C.; Wibowo, A. C.; Chung, D. Y.; Freeman, A. J.; Wessels, B. W.; Kanatzidis, M. G., Crystal Growth of the Perovskite Semiconductor $CsPbBr_3$: A New Material for High-Energy Radiation Detection. *Cryst. Growth Des.* **2013,** *13*, 2722-2727.

2. Lutz, H. D.; Beckenkamp, K.; Kellersohn, T.; Möller, H.; Peter, S., Neutron and X-Ray Structure Determination of Laurionite-Type Pb{O(H,D)}X, withX= Cl, Br, and I, Hydrogen Bonds to Lead(II) Ions as a Hydrogen-Bond Acceptor. *J. Solid State Chem.* **1996,** *124*, 155-161.